Permeability analyses and three dimensional imaging of interferon gamma-induced barrier disintegration in intestinal organoids

Bardenbacher, Marco ; Ruder, Barbara ; Britzen-Laurent, Nathalie ; Schmid, Benjamin ; Waldner, Maximilian ; Naschberger, Elisabeth ; Scharl, Michael ; Müller, Werner ; Günther, Claudia ; Becker, Christoph ; Stürzl, Michael ; Tripal, Philipp

Abstract: The aberrant regulation of the epithelial barrier integrity is involved in many diseases of the digestive tract, including inflammatory bowel diseases and colorectal cancer. Intestinal epithelial cell organoid cultures provide new perspectives for analyses of the intestinal barrier in vitro. However, established methods of barrier function analyses from two dimensional cultures have to be adjusted to the analysis of three dimensional organoid structures. Here we describe the methodology for analysis of epithelial barrier function and molecular regulation in intestinal organoids. Barrier responses to interferon-ɣ of intestinal organoids with and without epithelial cell-specific deletion of the interferon-ɣ-receptor 2 gene were used as a model system. The established method allowed monitoring of the kinetics of interferon-ɣ-induced permeability changes in living organoids. Proteolytic degradation and altered localization of the tight junction proteins claudin-2, -7, and - 15 was detected using confocal spinning disc microscopy with 3D reconstruction. Hessian analysis was used for quantification of re-localization of claudins. In summary, we provide a novel methodologic approach for quantitative analyses of intestinal epithelial barrier functions in the 3D organoid model.

DOI: https://doi.org/10.1016/j.scr.2019.101383

Stem Cell Research 35 (2019) 101383

Contents lists available at ScienceDirect

Stem Cell Research

journal homepage: www.elsevier.com/locate/scr

Permeability analyses and three dimensional imaging of interferon gamma-induced barrier disintegration in intestinal organoids

Marco Bardenbacher[a], Barbara Ruder[b], Nathalie Britzen-Laurent[a], Benjamin Schmid[e], Maximilian Waldner[b], Elisabeth Naschberger[a], Michael Scharl[c], Werner Müller[d], Claudia Günther[b], Christoph Becker[b], Michael Stürzl[a,*], Philipp Tripal[a,e]

[a] Division of Molecular and Experimental Surgery, Department of Surgery, Friedrich-Alexander-Universität (FAU) Erlangen-Nürnberg and Universitätsklinikum Erlangen, Translational Research Center, 91054 Erlangen, Germany
[b] Department of Medicine 1, Friedrich-Alexander-Universität (FAU) Erlangen-Nürnberg and Universitätsklinikum Erlangen, Kussmaul Campus, 91054 Erlangen, Germany
[c] Department of Gastroenterology und Hepatology, University Hospital Zürich, 8091 Zürich, Switzerland
[d] Bill Ford Chair in Cellular Immunology, Faculty of Biology, Medicine and Health, University of Manchester, Manchester M13 9PT, United Kingdom
[e] Optical Imaging Centre Erlangen (OICE), Friedrich-Alexander-Universität (FAU) Erlangen-Nürnberg, 91052 Erlangen, Germany

ARTICLE INFO

Keywords:
Inflammatory bowel disease
Interferon-gamma
Intestinal organoids
3D imaging
Permeability
Tight junction

ABSTRACT

The aberrant regulation of the epithelial barrier integrity is involved in many diseases of the digestive tract, including inflammatory bowel diseases and colorectal cancer. Intestinal epithelial cell organoid cultures provide new perspectives for analyses of the intestinal barrier *in vitro*. However, established methods of barrier function analyses from two dimensional cultures have to be adjusted to the analysis of three dimensional organoid structures. Here we describe the methodology for analysis of epithelial barrier function and molecular regulation in intestinal organoids. Barrier responses to interferon-γ of intestinal organoids with and without epithelial cell-specific deletion of the interferon-γ-receptor 2 gene were used as a model system. The established method allowed monitoring of the kinetics of interferon-γ-induced permeability changes in living organoids. Proteolytic degradation and altered localization of the tight junction proteins claudin-2, −7, and − 15 was detected using confocal spinning disc microscopy with 3D reconstruction. Hessian analysis was used for quantification of re-localization of claudins. In summary, we provide a novel methodologic approach for quantitative analyses of intestinal epithelial barrier functions in the 3D organoid model.

Key resources.

REAGENT or RESOURCE	SOURCE	IDENTIFIER
Antibodies		
rabbit anti-Claudin-2	Thermo Fisher Scientific	Cat#51–6100; RRID: AB_2533911
rabbit anti-Claudin-7	Thermo Fisher Scientific	Cat# 34–9100; RRID: AB_ 2,533,190
rabbit anti-Claudin-15	Thermo Fisher Scientific	Cat# 38–9200; RRID: AB_2533391
rabbit anti-cleaved-caspase-8	Cell Signaling	Cat#8592; RRID: AB_10891784
rabbit anti-phospho-Stat1	Cell Signaling	Cat#9167; RRID: AB_561284
goat anti-rabbit-Alexa 488	Thermo Fisher Scientific	Cat# A-11034; RRID: AB_2576217
Chemicals, Peptides, and Recombinant Proteins		
GM6001	Sigma	CC10; PubChem CID: 132519
Recombinant murine IFN-γ	Biolegend	Cat#575304
Recombinant human IFN-γ	Roche	Cat#11040596001
zVAD	Bachem	N-1560; CAS: 634911–81-2
Lucifer Yellow CH dilithium salt	Sigma	L0259; CAS: 67769–47-5
Experimental Models: Cell Lines		
Human T84 cells	ATCC	CCL-248
Experimental Models: Organoids		
Small intestine *M. musculus* C57/Bl6 IFNγR2^{wt}	The Jackson Laboratory	
Small intestine *M. Musculus* C57/Bl6 IFNγR2$^{\Delta IEC}$	(Lee et al., 2015)	
Oligonucleotides		
oligo-dT(18)	MWG	N/A
P1: TGACCCAAGACCAGTGGTC	This paper	N/A
P2: ATGAATTGGTCTGGGTCCTTTAG	This paper	N/A

* Corresponding author at: Division of Molecular and Experimental Surgery, Department of Surgery, Universitätsklinikum Erlangen, Translational Research Center, Schwabachanlage 12, 91054 Erlangen, Germany.
E-mail address: michael.stuerzl@uk-erlangen.de (M. Stürzl).

https://doi.org/10.1016/j.scr.2019.101383
Received 8 June 2018; Received in revised form 21 December 2018; Accepted 14 January 2019
Available online 07 February 2019

Software and Algorithms	
Graph Pad Prism	Version 4.0
Fiji	(Schindelin et al., 2012)

1. Introduction

The aberrant regulation of the epithelial barrier integrity is involved in many diseases of the digestive tract, including inflammatory bowel diseases (IBD) and colorectal cancer (CRC). Specifically for IBD the loss of intestinal barrier function leading to bacterial translocation and intestinal inflammation is thought to represent the initiating event of the disease (Zhang and Li, 2014). Epithelial cells are polarized cells with a basal and an apical side. Proteins of the tight junctions (TJ) and adjacent adherence junctions (AJ) constitute the apical junctional complex (AJC) in epithelial cells and are key structures for the regulation of barrier integrity (Yano et al., 2017; Lopez-Posadas et al., 2017). Accordingly, it has been suggested that TJ dysregulation may be an important trigger of IBD pathogenesis (Bojarski et al., 2004).

Inflammation can cause intestinal barrier dysfunction by inducing epithelial cell apoptosis (Gitter et al., 2001), transcriptional repression of TJ proteins (Mankertz et al., 2000), internalization of TJ proteins by endocytosis (Utech et al., 2010) and proteolytic degradation of TJ proteins (Bojarski et al., 2004). In parallel, there is increasing evidence that matrix metalloproteinases (MMPs) contribute to the pathogenesis of IBD, though the exact mechanisms of action are not yet fully understood (Meijer et al., 2007; Heimesaat et al., 2011; Nighot et al., 2015).

IFN-γ is highly up-regulated in mucosal tissues of IBD patients and in different murine colitis models (Funderburg et al., 2013; Ito et al., 2006; Oshima et al., 2001). Using the CRC cell line T84 it has been shown that IFN-γ can increase epithelial cell barrier permeability in the absence of apoptosis (Bruewer et al., 2003). This indicated that IFN-γ effects on the cell barrier may be based on impairment of the AJC.

Previously trans-well assays were used in order to investigate epithelial cell barrier functions. This approach involves two dimensional (2D) cell cultures seeded on permeable filters (Fig. 1A, upper). In the two dimensional model polarized exposure of a target receptor can be overcome by stimulation of cells from the apical and basal side. In addition, the recipient compartment of the penetrating substance is exactly defined by the size of the well, which allows reproducible determination of the concentrations of penetrating substances. Moreover, in 2D cell cultures the immunocytochemical detection of molecules and procedures to quantify localization changes at the molecular level are well established.

Recently intestinal organoids have been established as an improved *in-vitro*-model recapitulating closely cell differentiation processes and the crypt-villus structure of the intestine (1). However, research using these three dimensional (3D) structures requires the adaptation of available methods from 2D models. For example, polarized exhibition of a receptor solely to the inner side of organoids may hinder activation by respective cytokines (Fig. 1, lower right). Moreover, varying inner volumes of organoids can cause volume dependent variations in the concentrations of the penetrating substances in colorimetric or fluorometric detection procedures. Finally, whole mount immunocytological procedures are required for the detection of molecules of interest and available methods for quantification of localization changes have to be adapted for the specific models or procedures.

Here we established the methodology to quantitatively determine epithelial barrier functions in intestinal organoids and applied three dimensional reconstruction of confocal spinning disc z-stack images in order to analyse the impact of IFN-γ on TJ proteins.

2. Materials and methods

2.1. Animals

C57/Bl6 mice for the tissue specific knock out of the IFN-γR2 gene by the *Cre/loxP*-method have been described elsewhere (Lee et al., 2015). To obtain mice with a conditional IFN-γR2 knockout in the intestinal epithelium (IFN-γR2$^{\Delta IEC}$), these mice were crossed with mice harboring a Cre-recombinase under control of the villin promotor (The Jackson Laboratory, Bar Harbor, Maine, USA). The genotypes of the resulting mice were screened by polymerase chain reaction (PCR) analysis of genomic DNA isolated from tail biopsies.

2.2. Isolation and culture of intestinal mouse epithelial cells and organoids

Crypt isolation und cultivation was performed as described previously (Sato et al., 2009) with the following modifications. The small intestine from IFNγR2^{wt} or IFNγR2$^{\Delta IEC}$ mice was removed, washed with cold phosphate-buffered saline (PBS) and opened longitudinally. Villi were scraped off with a coverslip and discarded. The intestine was cut into small pieces, collected in cold PBS and washed by pipetting up and down. After sedimentation the supernatant was removed and the pellet was resuspended in cold PBS. This procedure was repeated until the supernatant became clear. Intestinal tissue pieces were incubated in PBS containing 2 mM EDTA for 30 min on ice while agitating. Afterwards tissue pieces were allowed to sediment, supernatant was discarded and replaced by cold PBS. Intestinal crypts were dissociated by vigorous pipetting. Upon sedimentation of aggregates, supernatant was collected and screened by microscopy. This was repeated until no more intestinal crypts were present in the supernatant. The fractions containing most of the intestinal crypts were passed through a cell strainer (70 µm pore size, Corning, Kaiserslautern, Germany) and centrifuged at 300 x g (5 min, 4 °C). Pelleted crypt structures were resuspended in a 1:1 mixture of Intesticult medium (Stemcell technologies, Köln, Germany) and growth factor reduced matrigel (Corning, NY, USA). Of this mixture 50 µl/well were distributed in 48-well plates (Thermo Fisher scientific, Dreieich, Germany). Upon polymerization of the Matrigel-Medium-Crypt mixture, Intesticult medium supplemented with 100 U/ml Penicillin, 100 µg/ml Streptomycin, 2.5 µg/ml amphotericin B, 2.05 mg/ml sodium deoxycholate (all Thermo Fisher scientific) and 20 µg/ml Gentamycin (Lonza, Basel Switzerland) was added (300 µl/well). Organoids were cultured at 37 °C in a 5% CO_2 atmosphere for at least 7 days before usage in experiments. Medium was replaced every 2–3 days and organoids were sub-cultivated at least once per week. For the experiments, organoids were treated for 48 h with 10 U/ml (0.4 ng/ml) recombinant murine IFN-γ (Biolegend, London, United Kingdom), 50 µM GM6001 dissolved in DMSO (both Sigma-Aldrich), 20 µM zVAD (Bachem, Bubendorf, Switzerland) alone, in combination or vehicle only. Medium was replaced every 24 h.

2.3. Organoid permeability assay

Organoids were plated in 8-well chamber slides (Ibidi, Planegg, Germany). After treatment, the assay was performed in a Leica TCS-SPE live cell observer (Leica, Wetzlar, Germany) at 37 °C with 5% CO_2. Upon beginning 1 mM lucifer yellow (Merck, Darmstadt, Germany) was added to the medium, organoids were imaged for 70 min by confocal microscopy with an interval of 5 min. To ensure the capability of imaged organoids to take up Lucifer yellow, EGTA (Merck) at a final concentration of 2 mM was added after the 70 min observation time. After EGTA was added, organoids were further imaged for 30 min. EGTA causes breakdown of the tight junctions by sequestering bivalent ions, independently of inflammatory stimuli. Densitometric analysis was performed using Leica LAS X Core software (Leica). For each time point, lucifer yellow fluorescence was quantified. Fluorescence intensity inside the organoid was normalized to the mean total

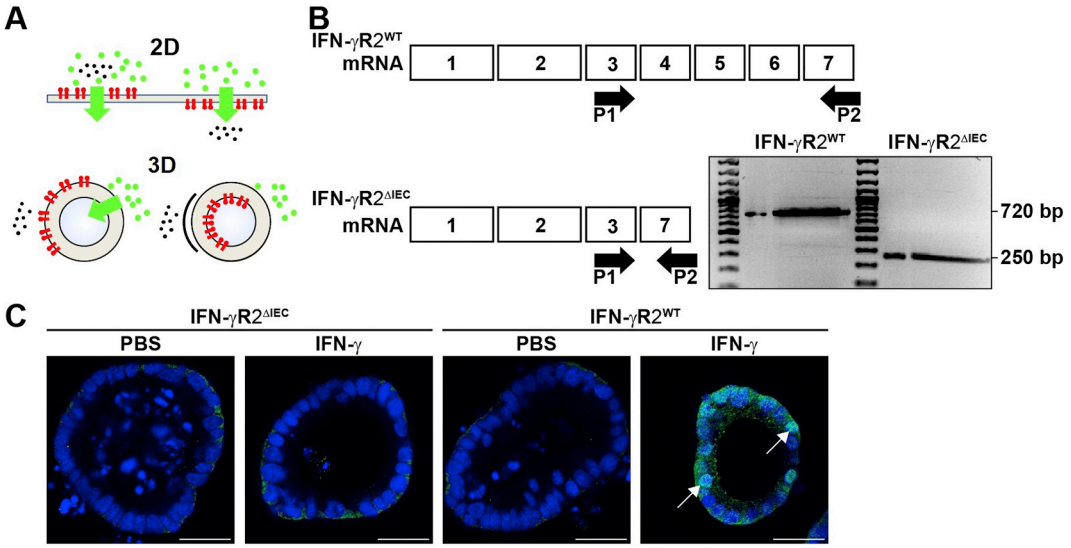

Fig. 1. 3D adaptation of barrier function analyses. (A) During barrier function analysis in 2D models polarized exposure of a target receptor (red) can be overcome by stimulation of cells from the apical and basal side (black dots). The recipient compartment of the penetrating substance is exactly defined by the size of the well, which allows reproducible determination of the concentrations of penetrating substances (green). Using 3D organoid structures polarized exhibition of a receptor solely to the inner side of organoids (lower right) may hinder activation by respective cytokines. Varying inner volumes of organoids may result in volume dependent variations in the concentrations of the penetrating substances in fluorometric detection procedures (green). (B) Schematic depiction of the IFN-γR2 locus in wild type (IFN-γR2^{WT}) and IFN-γR2 knock out (IFN-γR2$^{\Delta IEC}$) mice. Numbered boxes (1–7) indicate exons. LoxP sites in IFN-γR2^{WT} animals were present between exon 3/4 and exon 6/7. Binding sites of PCR primers (P1, P2) are indicated by arrows. RT-PCR of mRNA extracted from intestinal epithelial cells of IFN-γR2$^{\Delta IEC}$ and IFN-γR2^{WT} animals with P1 and P2 primers yielded PCR products with 250 bp and 720 bp respectively, indicating successful knock out of exons 4 to 6. (C) In order to investigate accessibility of the IFN-γR2 and to demonstrate specificity of activation of intestinal organoids from IFN-γR2$^{\Delta IEC}$ and IFN-γR2^{WT} animals were treated with IFN-γ (30 min). Nuclear, phosphorylated STAT-1 (green, arrows) was only induced by IFN-γ treatment in organoids of IFN-γR2^{WT} animals but not of IFN-γR2$^{\Delta IEC}$ animals as detected by indirect immunofluorescence. Nuclei were counter stained with DRAQ5 (blue). A central optical slice of an organoid is shown. Size bar = 25 µm. (For interpretation of the references to colour in this figure legend, the reader is referred to the web version of this article.)

fluorescence intensity (sum of three representative areas outside and inside the organoid). Only organoids which took up lucifer yellow after EGTA treatment were analysed.

2.4. Whole mount organoid immunofluorescence staining

Organoids were plated in 8-well chamber slides (Corning, New York, USA). After treatment, organoids were washed twice with cold PBS and fixed by incubation within neutrally buffered 4% paraformaldehyde (Merck) for 30 min at ambient temperature.

For immunocytochemical detection of claudin-2, claudin-7, claudin-15, caspase-8 or phospho-STAT-1 organoids were permeabilized after fixation in 0.5% Triton-X100 (Merck) diluted in Tris-buffered saline (TBS) for 30 min at ambient temperature or within precooled methanol for 10 min at −20 °C for phospho-Stat-1 staining. Specific binding of primary antibodies [rabbit anti-Claudin-2, rabbit anti-Claudin-7, rabbit anti-Claudin-15 all from Thermo Fisher Scientific (Waltham, MA, USA) and rabbit anti-cleaved-caspase-8 as well as rabbit anti-phospho-Stat1 from Cell Signaling (Leiden, Netherlands)] was achieved by incubating overnight at ambient temperature. After washing, incubation continued with a goat anti-rabbit secondary antibody, coupled to AlexaFluor-488 (Molecular Probes/Life technologies) for 7 h at ambient temperature. Nuclei were counterstained with Draq5 (Cell signaling) before organoids were mounted on glass slides within fluorescence mounting medium (Carl Roth, Karlsruhe, Germany). Confocal imaging was performed on a Leica TCS-SPE inverse microscope or a Zeiss Spinning Disc Axio Z1 live cell observer (Zeiss, Jena, Germany).

2.5. Organoid protein extraction

Medium was removed and organoids where harvested by vigorous pipetting with cold PBS. Organoids were centrifuged at 300 x g (5 min, 4 °C), washed twice with cold PBS and again centrifuged at 300 x g (5 min, 4 °C). Supernatants were discarded and organoids were resuspended in cold RIPA-buffer [50 mM tris-HCl, 150 mM NaCl, 0.1% sodium dodecyl sulfate, 0.5% sodium deoxycholate, 1% Nonident P-40, complete mini protease inhibitor cocktail (Roche Applied Science, Mannheim, Germany)]. Lysis was performed for 10 min on ice. After lysis, cell protein extracts were centrifuged at 20,000 x g (10 min, 4 °C). Supernatants were stored at −20 °C.

2.6. Cultivation of T84 cells

The human colorectal carcinoma cell line T84 (CCL-248) was purchased from ATCC (Manassas, Virginia, USA) and cultured in Dulbecco's modified Eagle's medium/Ham's medium with 2 mM glutamine and 10% FBS at 37 °C with 5% CO_2. When indicated, cells were treated with 100 U/ml (5 ng/ml) recombinant human IFN-γ (Roche Applied Science, Mannheim, Germany), GM6001 dissolved in DMSO (both Sigma-Aldrich) or respective amount of DMSO only. Cells were routinely tested for contamination with mycoplasma and tests were always negative. Short tandem repeat analysis was used to confirm the identity of the cells once a year (Stürzl et al., 2013).

2.7. Western blot analysis

Western blot analyses were performed as described previously (Britzen-Laurent et al., 2013). For the detection of 10 kDa claudin cleavage products, the procedure was modified as described previously (Britzen-Laurent et al., 2013). Detection of claudin-2, claudin-7, claudin-15 was performed using rabbit anti-claudin-2, rabbit anti-claudin-7, rabbit anti-claudin-15 antibodies (all Thermo Fisher Scientific) as primary antibodies and a goat anti-rabbit-horseradish-peroxidase–coupled secondary antibody (Dako, Hamburg, Germany).

2.8. Isolation of mRNA from mouse tissues and RT-PCR

Small intestine was isolated and flushed with ice cold PBS and collected in Trizol reagent (Thermo Fisher Scientific). Tissues were frozen at −80 °C and grinded for 10 min at 2000 rpm in a dismembrator (Braun, Melsungen, Germany). Total RNA was extracted according to the manufacturer's instructions. RNA concentration was determined photometrically (Nanodrop, VWR, Radnor, PA, USA) at λ = 260 nm, and RNA integrity was controlled by non-denaturating agarose gel electrophoresis. Reverse transcription was carried out in a total reaction volume of 20 µl with 1 µg total RNA, 200 U Superscript III reverse transcriptase (Thermo Fisher Scientific) and 0.1 µmol of an oligo-dT(18) primer (MWG, Ebersberg, Germany). The resulting cDNA was used to amplify the IFNγR2 cDNA for sequencing and to proof the *Cre/loxP*-mediated excision of Exon 4–6 in intestinal epithelia cells derived from IFNγR2$^{\Delta IEC}$ mice [primers used: P1 (fwd), TGACCCAAGACCAGT GGTC; P2 (rev), ATGAATTGGTCTGGGTCCTTTAG, see Fig. 1].

2.9. Hessian analysis of three dimensional image data

Z-stack data of confocal organoid images were reconstructed using Fiji (Schindelin et al., 2012) to obtain three dimensional representations of the organoid claudin localization. To quantify localization changes, for each voxel, the eigenvalues of the Hessian matrix of second order partial derivatives were calculated, which represent an orientation-independent measure for the degree of change along all three dimensions. Three high eigenvalues indicate the presence of blob-like structures, two high eigenvalues indicate tubular structures, while a single high eigenvalue indicates planar structures (Mosaliganti et al., 2012) that make up surfaces such as intact cell membranes. As a measure for the amount of intact membranes, which we also call surfaceness in the following, we therefore divide the mean of the strongest eigenvalue by the mean of the middle eigenvalue. These surfaceness values were calculated for each analysed organoid and mean values are displayed.

2.10. Statistical analysis

Statistical difference was calculated by two-tailed students *t*-Test using GraphPad Prism version 4.00 (GraphPad Software, San Diego, CA).

3. Results

3.1. IFN-γ increases epithelial barrier permeability in intestinal mouse organoids

In order to investigate the impact of IFN-γ on the integrity of the intestinal barrier, intestinal organoids were generated, from mice, lacking the IFN-γ-receptor 2 (IFN-γR2) in intestinal epithelial cells (IFN-γR2$^{\Delta IEC}$) and respective fl/fl control animals (IFN-γR2^{wt}) (Sato et al., 2009; Sato et al., 2011). The cell specific knock out of the IFN-γR2 gene was achieved by the *Cre/loxP*-system (Lakso et al., 1992) expressing the Cre-recombinase under control of the epithelial cell specific villin-promotor in mice, carrying two *loxP* sites within the gene coding for the IFN-γR2. In order to validate the gene knock out, RNA was extracted from the small intestine tissues of wild type and knock out animals. RT-PCR showed that IFN-γR2$^{\Delta IEC}$ animals expressed a truncated RNA of the IFN-γR2, lacking the exons 4, 5 and 6 (Fig. 1B). To investigate availability of the IFN-γR2 for IFN-γ added to the outside of organoids and to validate the functional impact of IFN-γR2 truncation, we analysed the activation of the signal transducer and activator of transcription 1 (STAT1) in organoid cultures. It is known that IFN-γ treatment induces dimerization and phosphorylation of STAT1 (Shuai et al., 1992). IFN-γ treatment increased the amount of phosphorylated nuclear STAT1 in intestinal organoids derived from wild type animals (Fig. 1C, arrows) but not in organoids from animals lacking the IFN-γR2 (IFN-γR2$^{\Delta IEC}$).

Epithelial cells in organoids are highly polarized (Fatehullah et al., 2013) and tight junctions prohibit permeation of Lucifer yellow 457 Da (LY) molecules (Fig. 2). In agreement with this, unstimulated organoids did not show intraluminal LY fluorescence after an exposure of 70 min (Fig. 2A, movie 1). In contrast, luminal uptake of LY was clearly visible in organoids derived from wild type mice (IFN-γR2^{WT} + IFN-γ), but not in the knock out animals (IFN-γR2$^{\Delta IEC}$, Fig. 2A, movie 1) upon stimulation with IFN-γ. In order to determine the kinetics of LY uptake, LY fluorescence signal intensity was measured within and outside the organoids every five minutes for an overall period of 70 min (Fig. 2B). In order to exclude permeability changes due to changes of surface to volume ratios upon organoid size variation, only organoids with comparable diameters were used for these experiments (Fig. 2C upper, 80 µm ± 20 µm). Subjecting all mouse intestinal organoids of the study (IFN-γR2^{WT}: n = 30, IFN-γR2$^{\Delta IEC}$: n = 29) to the permeability analysis LY penetration was significantly increased upon treatment with IFN-γ in wild type animals (Fig. 2C lower, IFN-γR2^{WT}). The lack of a functional IFN-γR2 prevented the luminal uptake of LY upon IFN-γ treatment (Fig. 2C lower, IFN-γR2 $^{\Delta IEC}$).

IFN-γ can induce apoptosis in epithelial cells in concentrations of 100 U/ml (Nava et al., 2011). In this study lower concentrations of IFN-γ (10 U/ml) were used, which did not affect organoid morphology after 48 h. In agreement with this the absence and presence of the apoptosis inhibitor ZVAD did not affect IFN-γ-induced permeability of the organoids (Fig. 2D). In order to identify apoptotic cells, the organoids were fixed with formalin after measuring the LY uptake and stained for activated caspase 8 (Fig. 2E). Only rarely single apoptotic cells were detected in the epithelial layers of the organoids irrespective whether they were treated with IFN-γ alone, simultaneously with ZVAD or left untreated (Fig. 2E, arrows). These findings indicated that increased organoid permeability in the presence of IFN-γ was not due to increased apoptosis.

3.2. IFN-γ induces MMP-dependent claudin fragmentation

Claudins are major components of the TJ. Within the intestinal TJ, claudin-2, −7 and − 15 are the predominantly present members of this protein family (Fujita et al., 2006; Tanaka et al., 2015). In order to identify whether modification of claudins may contribute to the IFN-γ-induced increase in epithelial barrier permeability, we analysed by Western blot the expression of claudins in organoids of wild type mice in the absence and presence of IFN-γ. Upon treatment with IFN-γ, the amounts of full-length claudin-2, −7 and − 15 proteins were reduced (Fig. 3A). This was accompanied by the appearance of 10 kDa cleavage fragments of all three claudins (Fig. 3A, upper panels). IFN-γ treatment had no impact on expression and proteolytic cleavage of the respective claudins in organoids from IFN-γR2$^{\Delta IEC}$ mice (Fig. 3A, lower panels).

Matrix metalloproteinases (MMPs) are commonly involved in inflammation associated tissue remodeling. In order to investigate the impact of MMPs in IFN-γ-induced claudin fragmentation we tested the inhibition of this effect by the broad-spectrum MMP inhibitor (galardin, GM6001) (Bendeck et al., 1996; Rawlings et al., 2014). Cleavage of claudin-2, −7 and − 15 was significantly repressed by GM6001 (Fig. 3A upper panels, B). Quantitative evaluation of signal intensities and the relative quantification of the cleaved and the full-length claudin confirmed that the cleavage product was significantly enriched in wild type mice-derived organoids treated with IFN-γ and repressed by the application of GM6001 (Fig. 3A upper panels, B).

The effect of IFN-γ treatment on claudin expression was confirmed in the human colon tumor cell line T84 for the human colon-associated claudin-7 (Fig. 3C, left panel) and claudin-2 (Fig. 3C, right panel). Treatment with IFN-γ for a period of 48 h decreased the expression of the full-length proteins and increased the appearance of 10 kDa cleavage products (Fig. 3C). IFN-γ induced cleavage of claudin-7 in T84 cells was inhibited by GM6001 in a concentration dependent manner

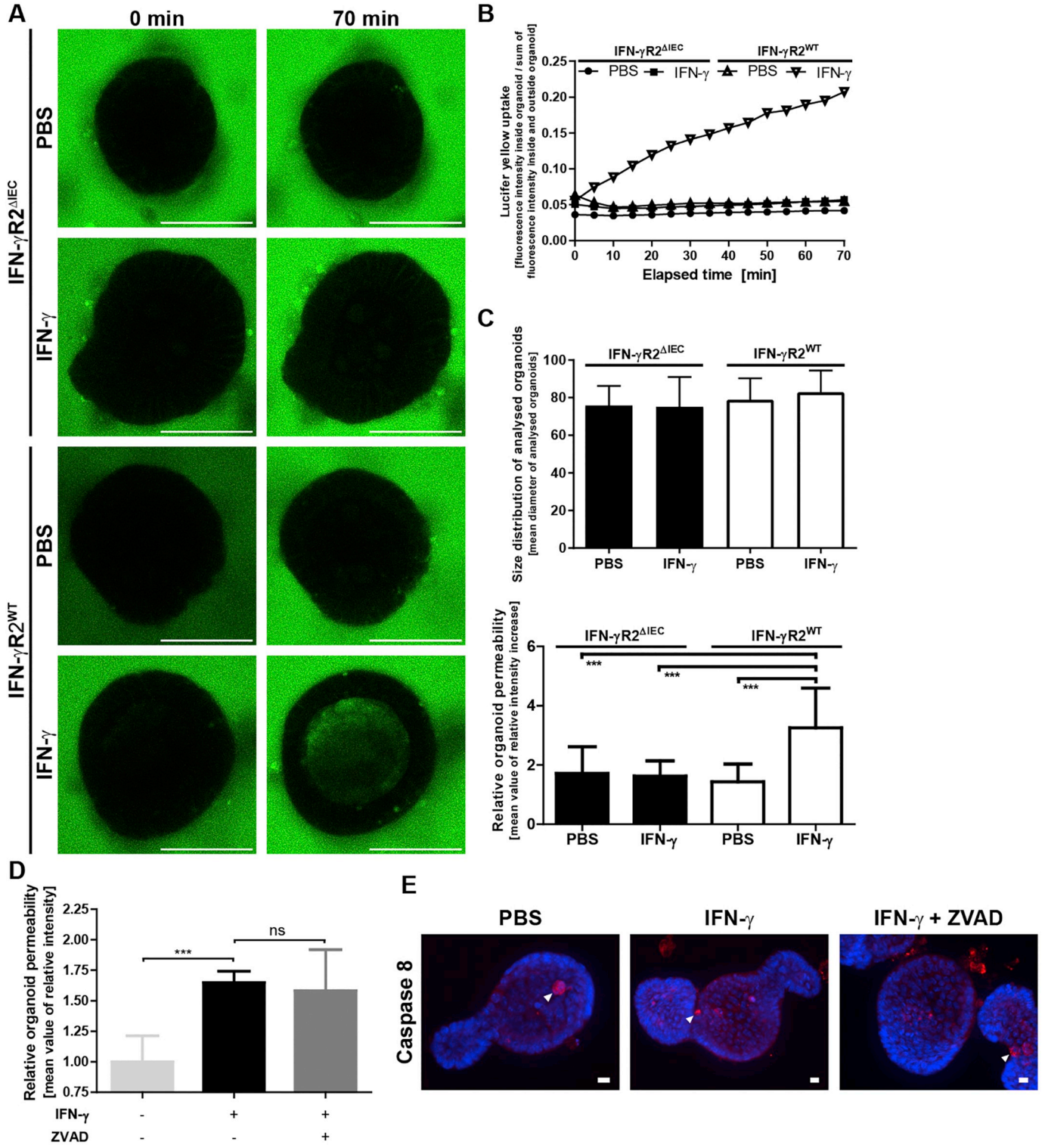

Fig. 2. IFN-γ induces breakdown of the epithelial barrier in mouse intestinal organoids. (A) Intestinal organoids from IFN-γR2^{WT} and IFN-γR2$^{\Delta IEC}$ were cultured in the absence (PBS) and presence of IFN-γ (IFN-γ) for 48 h. Upon addition of Lucifer yellow (457 Da) confocal fluorescent images were captured every 5 min for 70 min. Representative images at time point 0 min and 70 min are shown (green: Lucifer yellow, size bar = 50 μm). (B) Fluorescence was determined in the organoid lumen and outside of the organoid for the organoids depicted in A. Relative intensity values were calculated (fluorescence inside/outside + inside) and are shown for each time point. (C) Upper panel: only organoids with a diameter of 80 μm ± 20 μm were used. Mean values of the respective organoid diameters are shown (IFN-γR2^{WT}: $n = 30$, IFN-γR2$^{\Delta IEC}$: $n = 29$). The mean diameter values were not significantly different between the different groups by one-way ANOVA. Lower panel: The relative organoid permeability of IFN-γR2^{WT} and IFN-γR2$^{\Delta IEC}$ organoids was determined by dividing the relative fluorescence intensities obtained after 70 min by the minimal relative fluorescence intensities measured during the observation period. Each bar represents mean values, measured in 10 organoids derived from three independent experiments (IFN-γR2^{WT}: n = 30, IFN-γR2$^{\Delta IEC}$: n = 29). Only in IFN-γR2^{WT} organoids intestinal permeability is significantly increased after stimulation with IFN-γ. *** is equal to a p-value < .001 in the Student's t-test. (D) Organoids were cultured for 48 h in the presence of IFN-γ, IFN-γ + zVAD or left untreated (control). Upon addition of LY intraluminal LY fluorescence was measured (1 h, 5 min intervals). IFN-γ-induced uptake of LY was not reduced by zVAD. (E) After the experiment in (D) organoids were fixed and apoptosis was visualized by staining for activated effector caspase −8. Only fery few apoptotic cells (arrows) are visible under the different conditions. (size bar = 10 μm). (For interpretation of the references to colour in this figure legend, the reader is referred to the web version of this article.)

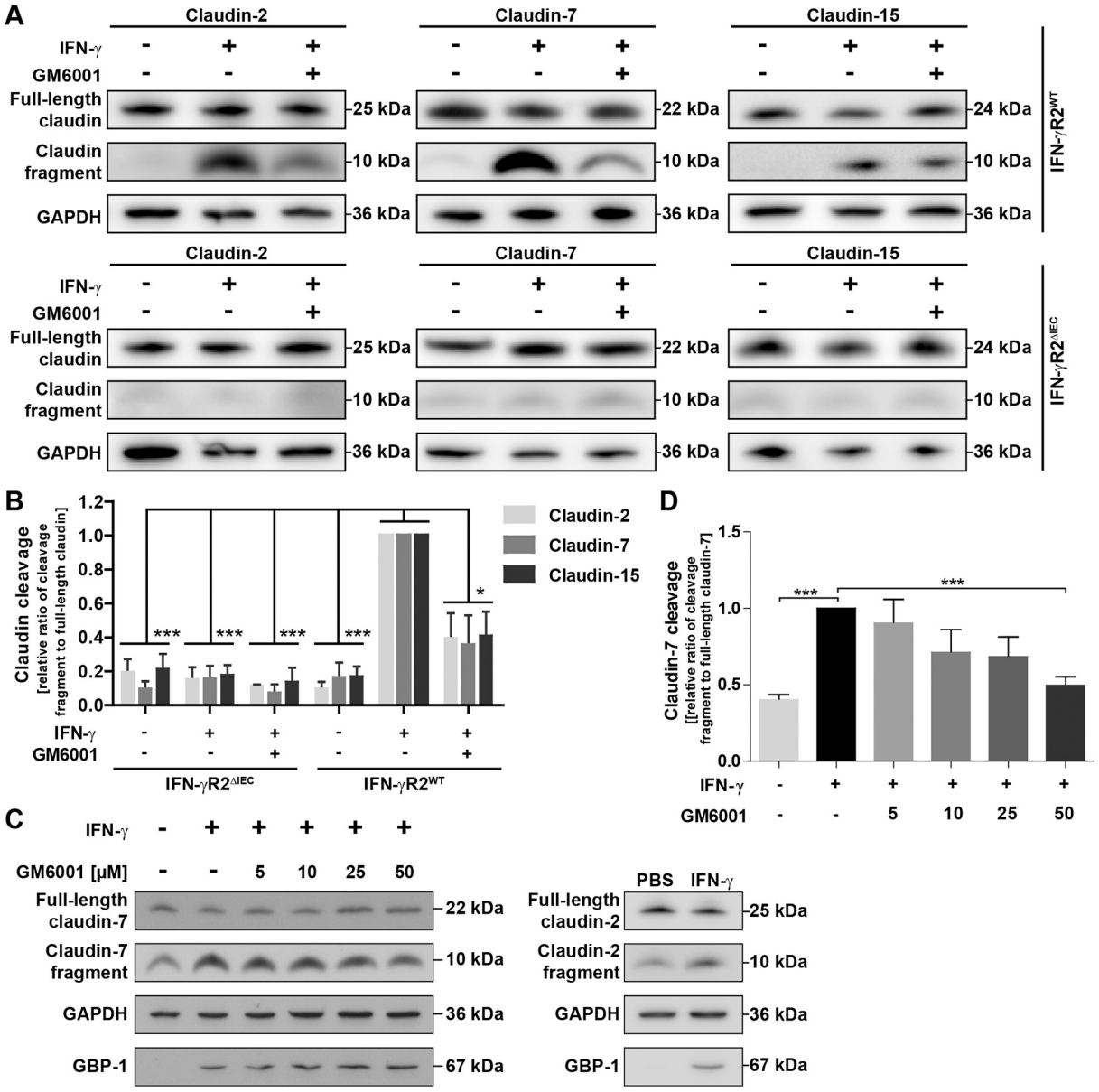

Fig. 3. Cleavage of intestinal barrier claudins is induced by IFN-γ in intestinal organoids and T84 cells. (A) Organoids from wild type (IFN-γR2^{WT}, upper panels) and IFN-γR2$^{\Delta IEC}$ (lower panels) mice were cultured in the presence of IFN-γ, IFN-γ + GM6001 or left untreated. Cell lysates of the respective organoids were analysed for the presence of the intestinal claudins (c-2, −7, −15). Intensities of the GAPDH signals demonstrate that identical amounts of protein lysates were loaded. Claudin-2, −7 and − 15 were present in all samples. The 10 kDa cleavage fragments are highly increased within lysates from IFN-γR2^{WT} organoids, treated with IFN-γ. Addition of GM6001 reduced the amount of the respective claudin cleavage fragments. (B) Quantification of claudin cleavage. Intensities of the Western blot signals from full-length claudin-2, −7, −15 and the respective cleavage fragments were quantified by densitometry. The results are depicted as the relative ratios of the 10 kDa cleavage fragment to the respective full-length protein. The relative intensity values of the organoids, treated with IFN-γ were set to one. Cleavage of claudin-2, −7 and − 15 was significantly induced upon IFN-γ treatment. *P*-values < .001 (***), Student's t-test. Inhibition of cleavage by GM6001 is significant for each claudin analysed. P-values < .05 (*), Student's t-test. (C) Proteolytic cleavage of claudin-7 (left panel) and claudin-2 (right panel) is induced upon IFN-γ treatment in T84 cells. GM6001 treatment of T84 cells inhibits IFN-γ-induced cleavage of claudin-7. T84 cells were grown in the absence (−) or presence (+) of 100 U/ml IFN-γ for 48 h and GM6001 was added at concentrations of 5, 10, 25 or 50 μM. Claudin expression was analysed by Western blot. The GAPDH signal confirmed equal loading of proteins. Induction of GBP-1 expression demonstrated successful stimulation of the cells with IFN-γ. Full length and the 10 kDa cleavage fragments are depicted for claudin-7 and claudin-2. (D) Quantification of claudin-7 cleavage inhibition by GM6001. The results are depicted as the relative ratios of the 10 kDa fragment to full-length claudin-7. The values of the cells, treated with IFN-γ were set to one. Cleavage of claudin-7 upon IFN-γ stimulation was significantly reduced after treatment with GM6001 in a dose dependent manner. P-values < .001 (***), Student's t-test.

(Fig. 3C, left panel) as further demonstrated by quantification of the Western blot signals (Fig. 3D). Stimulation of T84 cells with IFN-γ was confirmed by the increased expression of the IFN-γ-induced guanylate-binding-protein-1 (GBP-1) (Fig. 3C)(Guenzi et al., 2001; Lubeseder-Martellato et al., 2002).

3.3. IFN-γ induces MMP-dependent relocalization of claudins in intestinal organoids

Immunofluorescence detection at the single cell level showed that the signals for claudin-2 and -15 concentrated at the apical side of epithelial cells forming a ring like structure around the lumen of wild type organoids (Fig. 4A, PBS, arrows, 3-dimensional reconstruction (3-

DR) see supplementary information 3-DR 1 and 3-DR 2). In contrast, claudin-7 was evenly distributed from the basal to the apical side of the epithelial cell-cell contact areas (Fig. 4A, PBS, arrows, see supplementary information 3-DR 3). Upon stimulation with IFN-γ, the localization of claudin-2, −7 and − 15 changed profoundly. Specifically, the ring like apical structures of claudin-2 and -15 were resolved (Fig. 4A, red arrows, see supplementary information 3-DR 4 and 3-DR 5) and the two claudins produced granular intracytoplasmic staining signals (Fig. 4A, yellow arrows). Similarly, claudin-7 was shifted towards aggregates on the apical side of the cells (Fig. 4A, yellow arrows, see supplementary information 3-DR 6). The addition of GM6001 to IFN-γ-treated wild type organoids partially restored the apical ring like presentation of claudin-2 and -15 and the localization of claudin-7 at the epithelial cell contact areas (Fig. 4A, arrows, see supplementary information 3-DR 7–3-DR 9, arrows). In organoids derived from IFN-γR2$^{\Delta IEC}$ animals claudin localizations were not altered in the presence of IFN-γ, confirming that the changes observed in wild type organoids were specifically induced by IFN-γ signaling *via* its receptor (Fig. 4B).

3.4. IFN-γ induced claudin destruction and conservation in the presence of an MMP inhibitor can be quantified by image analysis of three dimensional microscopy data

To confirm the structural claudin changes in the presence of IFN-γ and/or GM6001, three dimensional image data were quantified by calculating a surfaceness measure based on Hessian analysis (Mosaliganti et al., 2012). Upon stimulation of organoids with IFN-γ, the surfaceness values of claudin-2, −7 and − 15 were increased in organoids derived from control animals and the simultaneous addition of GM6001 reduced this increase (Fig. 5). In organoids derived from IFN-γR2$^{\Delta IEC}$ animals, the effect of IFN-γ and GM6001 could quantitatively not be determined (data not shown).

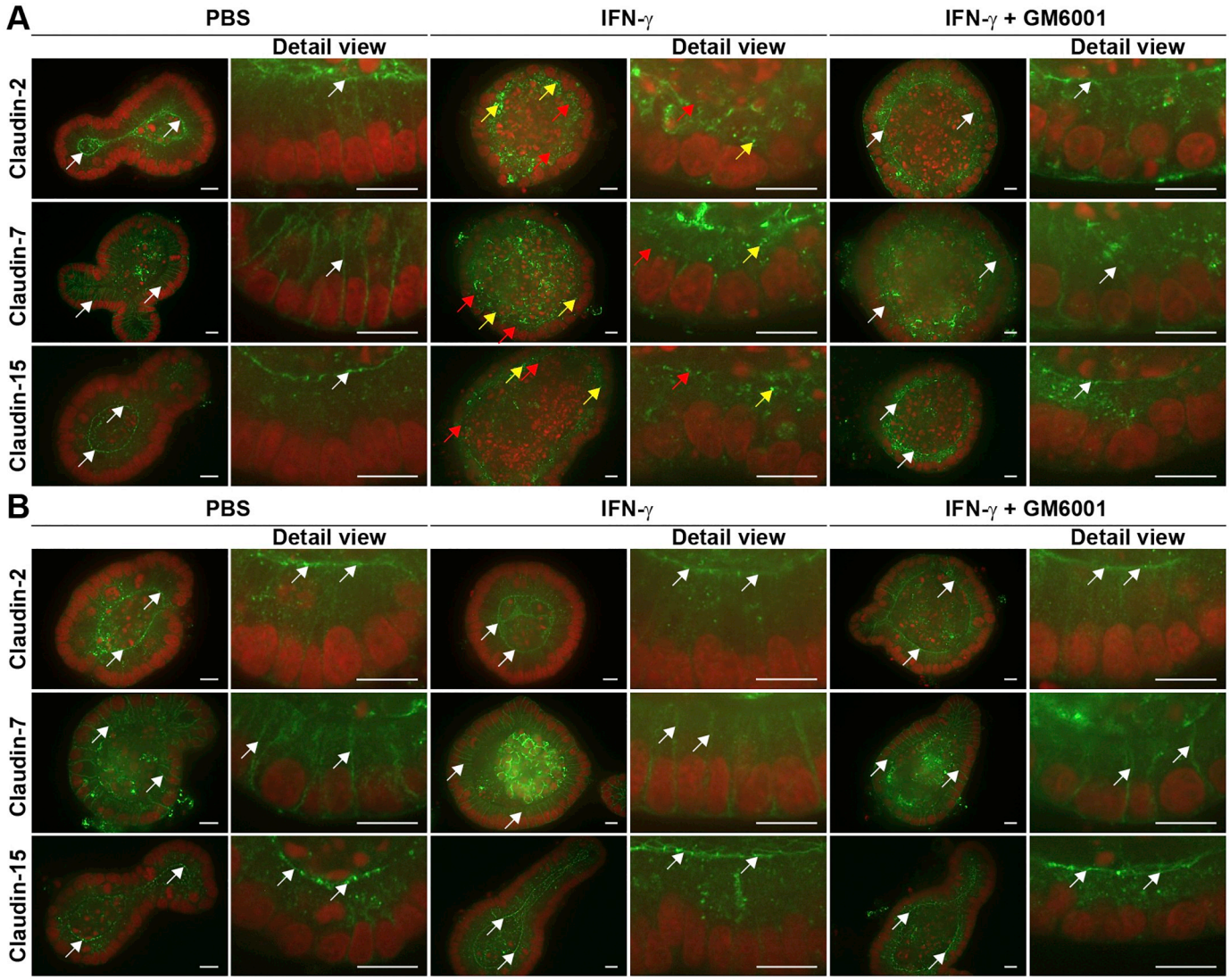

Fig. 4. IFN-γ-induced cleavage alters cellular localization of claudins. Mouse organoids derived from (A) wildtype (IFN-γR2^{WT}) and (B) IFN-γR2$^{\Delta IEC}$ mice were cultivated in the presence of IFN-γ, IFN-γ and GM6001 or left untreated (PBS). 48 h after stimulation, organoids were fixed with PFA and claudin-2, −7 and − 15 were stained by indirect immunofluorescence (green) and nuclei were counterstained by Draq5 (red). Within organoids, claudin-2, −7 and − 15 localize within defined structures (white arrows). While claudin-2 and -15 are enriched at the apical cell-cell contacts surrounding the organoid lumen, claudin-7 localizes along the whole epithelial cell-cell contact area. In IFN-γR2^{WT} organoids (A) the treatment with IFN-γ destroyed the regular localization of claudin-2, −7 and − 15. The apical lining of claudin-2 and -15 structures became discontinuous (red arrows) and intracellular aggregates of claudin-2, −7 and − 15 were apparent (yellow arrow). The addition of galardin (GM6001) partly reversed IFN-γ induced changes by reinstalling claudin-2 and -15 at the apical luminal ring structure (arrow) and claudin-7 in the cell-cell contact area (arrow). (B) In organoids from IFN-γR2$^{\Delta IEC}$ mice neither treatment with IFN-γ nor galardin changed the localization of c-2, c-7 and c-15. The scale bar represents 10 μm. (For interpretation of the references to colour in this figure legend, the reader is referred to the web version of this article.)

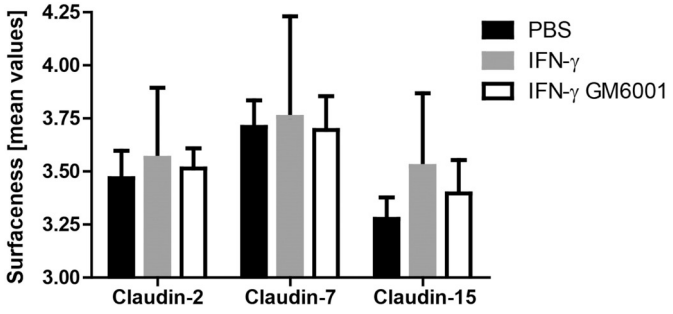

Fig. 5. IFN-γ-induced changes of claudin localization can be quantified from 3D image data. Intestinal organoids derived from wildtype (IFN-γR2^{WT}) mice were cultivated in the presence of IFN-γ (grey bars), IFN-γ and GM6001 (white bars) or left untreated (PBS, black bars). 48 h after stimulation, organoids were fixed with PFA and claudins-2, −7 and − 15 were stained by indirect immunofluorescence. Claudin fluorescence was imaged by confocal microscopy and z-sectioning. *Z*-stack images were used to reconstruct the claudin localization in 3D (supplementary 3-DR images) and Hessian analysis was applied to quantify changes in claudin localization. Mean of surfaceness values and SD obtained from $n \geq 6$ organoids are shown.

4. Discussion

Polarity and barrier integrity are important features of the intestinal epithelium. Both of these functions require a functional apical junctional complex (Yano et al., 2017) and are present in stem cell dependent organoid cultures of the small intestine. Here, we described the methodology to analyse IFN-γ-induced permeability changes in small intestinal organoids. Our results show that mini guts are a valuable *in-vitro*-model to investigate intestinal barrier functions. This finding is in agreement with studies from others investigating nutrient and drug transport in intestinal organoids as well as tight junction composition in organoids of different intestinal cell types (Zietek et al., 2015; Pearce et al., 2018). In addition, forskolin treatment of organoids induces swelling through CFTR-dependent ion and water transport into the lumen, which may be used as an alternative readout of barrier defects (Boj et al., 2017). All of these models including ours investigated the outside-in permeation of the analytic dye. Barrier penetration from the inside to outside direction was investigated recently, using human pluripotent stem cell-derived intestinal organoids and microinjection of fluorescently-labelled dextran (Hill et al., 2017). However, this approach is technically more demanding and does not allow analyses of several different organoids in parallel as compared to the outside-in approach used here. We demonstrated that in our model permeability changes were specifically induced by IFN-γ and did not appear in organoids obtained from mice lacking the IFN-γR2 in intestinal epithelial cells.

IFN-γ can induce apoptosis in epithelial cells (Nava et al., 2011). However, low concentrations of IFN-γ were used in our study, which did not induce apoptosis to a level that may explain the observed changes in permeability. Alternatively, it has been reported that inflammatory cytokines can regulate TJ expression at the transcriptional level (Mankertz et al., 2000). In agreement with this finding and our observations it was shown that IFN-γ can induce breakdown of the intestinal barrier independently of apoptosis (Bruewer et al., 2003). Based on these findings it was suggested that IFN-γ may have regulatory impact on the expression of TJ proteins in epithelial cells. However, the expression levels of claudin-2, −7 and − 15 in intestinal organoids were not significantly different in the presence and absence of IFN-γ. Interestingly, we now identified an IFN-γ-induced, 10 kDa degradation product for all claudins analysed. The appearance of the cleavage product was inversely related to a decrease of the full-length claudin proteins. In agreement with a previous study (Willemsen et al., 2005) we could confirm that IFN-γ treatment causes also in the human T84 cell line processing of claudin-2 into a 10 kDa fragment and we showed that this also applied for claudin-7, which again confirms the reliability of measuring intestinal barrier breakdown in small intestinal organoids.

The presence of GM6001 counteracted the IFN-γ induced proteolytic processing of claudins, suggesting that MMPs may catalyse this step. Both, the activity of serine- and matrixmetallo-proteinases are increased in colitis (Tarlton et al., 2000). This finding is in line with reports showing that MMPs are induced by IFN-γ (Malemud, 2017) and are present in increased concentrations in IBD (Baugh et al., 1999). The claudin antibodies used here are binding to the C-termini of the claudin proteins, which are localized in the cytoplasm. This suggests that the proteolytic 10 kDa claudin fragments are released by intracellular cleavage. In this framework it is of interest that recent findings pointed to intracellular effects of MMPs (Jobin et al., 2017), which previously were predominantly suspected to act on extracellular matrix proteins.

The claudin C-termini are connecting the TJ to the actin cytoskeleton. Disruption of this connection has been shown to be sufficient for TJ weakening (Bojarski et al., 2004), supporting that IFN-γ-induced claudin cleavage may be sufficient to cause barrier disintegration in intestinal organoids.

The automated quantification of structural claudin changes induced by IFN-γ and GM6001 confirmed the visual changes from three dimensional images and claudin destruction observed by Western blot. However, the high biological variability, expressed in the diversity of structure and size of individual organoids also within each group, caused the high variances visible in Fig. 5. Accordingly, the tendency of the mean reflects our findings (a degradation of Claudin structure under IFN-γ, which is rescued in the presence of GM6001), but a much higher sample number will be required to achieve statistical significance. These findings indicate that proteolytic remodeling of Claudins contributes to IFN-γ-induced permeability changes in intestinal organoids, but also points to the fact that additional mechanisms are involved, which need further investigation.

In summary, our study describes the methodology for analyses of epithelial barrier functions in intestinal organoids. Intestinal organoids closely resembling the cellular differentiation patterns in the intestine are a highly relevant model system for analyses of the epithelial cell barriers. Intestinal organoids in combination with modern microscopic techniques and bioinformatics analyses of 3D image data open new avenues for analyses of the regulation of intestinal barrier functions in physiologic processes and diseases *in vitro*.

Supplementary data to this article can be found online at https://doi.org/10.1016/j.scr.2019.101383.

Acknowledgements

This work was supported by grants from the German Research Foundation (DFG) [KFO257, project 4 to M.S. and M.W. and project 1 to C.B.; FOR2438, project 2 to MS and E.N and project 5 to C.B.; SFB1181 project C05 to C.B.; TRR241, project A06 to M.B.-L. and M.S.; BR5196/2-1 to N.B.-L. and BE3686/2 to C.B.]; the Interdisciplinary Center for Clinical Research (IZKF) of the Clinical Center Erlangen (to M.S., E.N. and M.B.), the W. Lutz Stiftung (to M.S.) and the Forschungsstiftung Medizin of the Clinical Center Erlangen (to M.S.). The present work was performed in (partial) fulfillment of the requirements for obtaining the degree “Dr. med.” of Marco Bardenbacher.

Author contributions

M.B., M.S. and P.T. designed the experiments; M.B., B.R. and P.T. performed the experiments; M.B., N. B.-L., B.S., E.N., M.S., M.Sch and P.T. analysed the data; N. B.-L., C.G., M.W., W.M. and C.B. provided key reagents; and M.B., P.T. and M.S. wrote the manuscript. All of the authors approved the final manuscript.

Conflict of interest

The authors declare no conflict of interest.

References

Baugh, M.D., Perry, M.J., Hollander, A.P., Davies, D.R., Cross, S.S., Lobo, A.J., Taylor, C.J., Evans, G.S., 1999. Matrix metalloproteinase levels are elevated in inflammatory bowel disease. Gastroenterology 117, 814–822.

Bendeck, M.P., Irvin, C., Reidy, M.A., 1996. Inhibition of matrix metalloproteinase activity inhibits smooth muscle cell migration but not neointimal thickening after arterial injury. Circ. Res. 78, 38–43.

Boj, S.F., Vonk, A.M., Statia, M., Su, J., Vries, R.R., Beekman, J.M., Clevers, H., 2017. Forskolin-induced swelling in intestinal organoids: an in vitro assay for assessing drug response in cystic fibrosis patients. J. Visualized Exp. JoVE 120, e55159. https://doi.org/10.3791/55159.

Bojarski, C., Weiske, J., Schoneberg, T., Schroder, W., Mankertz, J., Schulzke, J.D., Florian, P., Fromm, M., Tauber, R., Huber, O., 2004. The specific fates of tight junction proteins in apoptotic epithelial cells. J. Cell Sci. 117, 2097–2107.

Britzen-Laurent, N., Lipnik, K., Ocker, M., Naschberger, E., Schellerer, V.S., Croner, R.S., Vieth, M., Waldner, M., Steinberg, P., Hohenadl, C., Stürzl, M., 2013. GBP-1 acts as a tumor suppressor in colorectal cancer cells. Carcinogenesis 34, 153–162.

Bruewer, M., Luegering, A., Kucharzik, T., Parkos, C.A., Madara, J.L., Hopkins, A.M., Nusrat, A., 2003. Proinflammatory cytokines disrupt epithelial barrier function by apoptosis-independent mechanisms. J. Immunol. 171, 6164–6172.

Fatehullah, A., Appleton, P.L., Nathke, I.S., 2013. Cell and tissue polarity in the intestinal tract during tumourigenesis: cells still know the right way up, but tissue organization is lost. Philos. Trans. R. Soc. Lond. Ser. B Biol. Sci. 368, 20130014.

Fujita, H., Chiba, H., Yokozaki, H., Sakai, N., Sugimoto, K., Wada, T., Kojima, T., Yamashita, T., Sawada, N., 2006. Differential expression and subcellular localization of claudin-7, -8, -12, -13, and -15 along the mouse intestine. J. Histochem. Cytochem. Off. J. Histochem. Soc. 54, 933–944.

Funderburg, N.T., Stubblefield Park, S.R., Sung, H.C., Hardy, G., Clagett, B., Ignatz-Hoover, J., Harding, C.V., Fu, P., Katz, J.A., Lederman, M.M., Levine, A.D., 2013. Circulating CD4(+) and CD8(+) T cells are activated in inflammatory bowel disease and are associated with plasma markers of inflammation. Immunology 140, 87–97.

Gitter, A.H., Wullstein, F., Fromm, M., Schulzke, J.D., 2001. Epithelial barrier defects in ulcerative colitis: characterization and quantification by electrophysiological imaging. Gastroenterology 121, 1320–1328.

Guenzi, E., Töpolt, K., Cornali, E., Lubeseder-Martellato, C., Jörg, A., Matzen, K., Zietz, C., Kremmer, E., Nappi, F., Schwemmle, M., Hohenadl, C., Barillari, G., Tschachler, E., Monini, P., Ensoli, B., Stürzl, M., 2001. The helical domain of GBP-1 mediates the inhibition of endothelial cell proliferation by inflammatory cytokines. EMBO J. 20, 5568–5577.

Heimesaat, M.M., Dunay, I.R., Fuchs, D., Trautmann, D., Fischer, A., Kuhl, A.A., Loddenkemper, C., Batra, A., Siegmund, B., Krell, H.W., Bereswill, S., Liesenfeld, O., 2011. Selective gelatinase blockage ameliorates acute DSS colitis. Eur. J. Microbiol. Immunol. 1, 228–236.

Hill, D.R., Huang, S., Tsai, Y.H., Spence, J.R., Young, V.B., 2017. Real-time measurement of epithelial barrier permeability in human intestinal organoids. J. Visualized Exp. JoVE 130, e56960. https://doi.org/10.3791/56960.

Ito, R., Shin-Ya, M., Kishida, T., Urano, A., Takada, R., Sakagami, J., Imanishi, J., Kita, M., Ueda, Y., Iwakura, Y., Kataoka, K., Okanoue, T., Mazda, O., 2006. Interferon-gamma is causatively involved in experimental inflammatory bowel disease in mice. Clin. Exp. Immunol. 146, 330–338.

Jobin, P.G., Butler, G.S., Overall, C.M., 2017. New intracellular activities of matrix metalloproteinases shine in the moonlight. Biochim. Biophys. Acta 1864, 2043–2055.

Lakso, M., Sauer, B., Mosinger Jr., B., Lee, E.J., Manning, R.W., Yu, H., Mulder, K.L., Westphal, H., 1992. Targeted oncogene activation by site-specific recombination in transgenic mice. Proc. Natl. Acad. Sci. U. S. A. 89, 6232–6236.

Lee, H.M., Fleige, A., Forman, R., Cho, S., Khan, A.A., Lin, L.L., Nguyen, D.T., O'Hara-Hall, A., Yin, Z., Hunter, C.A., Muller, W., Lu, L.F., 2015. IFNgamma signaling endows DCs with the capacity to control type I inflammation during parasitic infection through promoting T-bet+ regulatory T cells. PLoS Pathog. 11, e1004635.

Lopez-Posadas, R., Stürzl, M., Atreya, I., Neurath, M.F., Britzen-Laurent, N., 2017. Interplay of GTPases and cytoskeleton in cellular barrier defects during gut inflammation. Front. Immunol. 8, 1240.

Lubeseder-Martellato, C., Guenzi, E., Jörg, A., Töpolt, K., Naschberger, E., Kremmer, E., Zietz, C., Tschachler, E., Hutzler, P., Schwemmle, M., Matzen, K., Grimm, T., Ensoli, B., Stürzl, M., 2002. Guanylate-binding protein-1 expression is selectively induced by inflammatory cytokines and is an activation marker of endothelial cells during inflammatory diseases. Am. J. Pathol. 161, 1749–1759.

Malemud, C.J., 2017. Matrix Metalloproteinases and Synovial Joint Pathology, Progress in Molecular Biology and Translational Science. 148. pp. 305–325.

Mankertz, J., Tavalali, S., Schmitz, H., Mankertz, A., Riecken, E.O., Fromm, M., Schulzke, J.D., 2000. Expression from the human occludin promoter is affected by tumor necrosis factor alpha and interferon gamma. J. Cell Sci. 113 (Pt 11), 2085–2090.

Meijer, M.J., Mieremet-Ooms, M.A., van Hogezand, R.A., Lamers, C.B., Hommes, D.W., Verspaget, H.W., 2007. Role of matrix metalloproteinase, tissue inhibitor of metalloproteinase and tumor necrosis factor-alpha single nucleotide gene polymorphisms in inflammatory bowel disease. World J. Gastroenterol. 13, 2960–2966.

Mosaliganti, K.R., Noche, R.R., Xiong, F., Swinburne, I.A., Megason, S.G., 2012. ACME: automated cell morphology extractor for comprehensive reconstruction of cell membranes. PLoS Comput. Biol. 8, e1002780.

Nava, P., Capaldo, C.T., Koch, S., Kolegraff, K., Rankin, C.R., Farkas, A.E., Feasel, M.E., Li, L., Addis, C., Parkos, C.A., Nusrat, A., 2011. JAM-A regulates epithelial proliferation through Akt/beta-catenin signalling. EMBO Rep. 12, 314–320.

Nighot, P., Al-Sadi, R., Rawat, M., Guo, S., Watterson, D.M., Ma, T., 2015. Matrix metalloproteinase 9-induced increase in intestinal epithelial tight junction permeability contributes to the severity of experimental DSS colitis. Am. J. Physiol. Gastrointest. Liver Physiol. 309, G988–G997.

Oshima, T., Laroux, F.S., Coe, L.L., Morise, Z., Kawachi, S., Bauer, P., Grisham, M.B., Specian, R.D., Carter, P., Jennings, S., Granger, D.N., Joh, T., Alexander, J.S., 2001. Interferon-gamma and interleukin-10 reciprocally regulate endothelial junction integrity and barrier function. Microvasc. Res. 61, 130–143.

Pearce, S.C., Al-Jawadi, A., Kishida, K., Yu, S., Hu, M., Fritzky, L.F., Edelblum, K.L., Gao, N., Ferraris, R.P., 2018. Marked differences in tight junction composition and macromolecular permeability among different intestinal cell types. BMC Biol. 16, 19.

Rawlings, N.D., Waller, M., Barrett, A.J., Bateman, A., 2014. MEROPS: the database of proteolytic enzymes, their substrates and inhibitors. Nucleic Acids Res. 42, D503–D509.

Sato, T., Vries, R.G., Snippert, H.J., van de Wetering, M., Barker, N., Stange, D.E., van Es, J.H., Abo, A., Kujala, P., Peters, P.J., Clevers, H., 2009. Single Lgr5 stem cells build crypt-villus structures in vitro without a mesenchymal niche. Nature 459, 262–265.

Sato, T., Stange, D.E., Ferrante, M., Vries, R.G., Van Es, J.H., Van den Brink, S., Van Houdt, W.J., Pronk, A., Van Gorp, J., Siersema, P.D., Clevers, H., 2011. Long-term expansion of epithelial organoids from human colon, adenoma, adenocarcinoma, and Barrett's epithelium. Gastroenterology 141, 1762–1772.

Schindelin, J., Arganda-Carreras, I., Frise, E., Kaynig, V., Longair, M., Pietzsch, T., Preibisch, S., Rueden, C., Saalfeld, S., Schmid, B., Tinevez, J.Y., White, D.J., Hartenstein, V., Eliceiri, K., Tomancak, P., Cardona, A., 2012. Fiji: an open-source platform for biological-image analysis. Nat. Methods 9, 676–682.

Shuai, K., Schindler, C., Prezioso, V.R., Darnell Jr., J.E., 1992. Activation of transcription by IFN-gamma: tyrosine phosphorylation of a 91-kD DNA binding protein. Science 258, 1808–1812.

Stürzl, M., Gaus, D., Dirks, W.G., Ganem, D., Jochmann, R., 2013. Kaposi's sarcoma-derived cell line SLK is not of endothelial origin, but is a contaminant from a known renal carcinoma cell line. Int. J. Cancer 132, 1954–1958.

Tanaka, H., Takechi, M., Kiyonari, H., Shioi, G., Tamura, A., Tsukita, S., 2015. Intestinal deletion of Claudin-7 enhances paracellular organic solute flux and initiates colonic inflammation in mice. Gut 64, 1529–1538.

Tarlton, J.F., Whiting, C.V., Tunmore, D., Bregenholt, S., Reimann, J., Claesson, M.H., Bland, P.W., 2000. The role of up-regulated serine proteases and matrix metalloproteinases in the pathogenesis of a murine model of colitis. Am. J. Pathol. 157, 1927–1935.

Utech, M., Mennigen, R., Bruewer, M., 2010. Endocytosis and recycling of tight junction proteins in inflammation. J Biomed Biotechnol (2010), 484987.

Willemsen, L.E., Hoetjes, J.P., van Deventer, S.J., van Tol, E.A., 2005. Abrogation of IFN-gamma mediated epithelial barrier disruption by serine protease inhibition. Clin. Exp. Immunol. 142, 275–284.

Yano, T., Kanoh, H., Tamura, A., Tsukita, S., 2017. Apical cytoskeletons and junctional complexes as a combined system in epithelial cell sheets. Ann. N. Y. Acad. Sci. 1405, 32–43.

Zhang, Y.Z., Li, Y.Y., 2014. Inflammatory bowel disease: pathogenesis. World J. Gastroenterol. 20, 91–99.

Zietek, T., Rath, E., Haller, D., Daniel, H., 2015. Intestinal organoids for assessing nutrient transport, sensing and incretin secretion. Sci. Rep. 5, 16831.